Available online at www.sciencedirect.com
ScienceDirect
International Journal of Thermal Sciences 47 (2008) 668–679
International Journal of Thermal Sciences
www.elsevier.com/locate/ijts

Influence of a horizontal magnetic field on the natural convection of paramagnetic fluid in a cube heated and cooled from two vertical side walls

Tomasz Bednarz [a,b,*], Elzbieta Fornalik [c], Hiroyuki Ozoe [b], Janusz S. Szmyd [c], John C. Patterson [a], Chengwang Lei [a]

[a] *School of Engineering, James Cook University, Townsville, Queensland 4811, Australia*
[b] *Kyushu University, Fukuoka, Japan*
[c] *AGH University of Science and Technology, Krakow, Poland*

Received 8 January 2007; received in revised form 18 June 2007; accepted 19 June 2007

Available online 6 August 2007

Abstract

A cube was filled with an aqueous solution of glycerol with the addition of gadolinium nitrate hexahydrate to make the working fluid paramagnetic. A very small amount of liquid crystal slurry was then added in order to visualize the local temperature inside the enclosure. One vertical wall of the cube was uniformly heated by nichrome wire from a DC power supply while the opposite one was cooled by cold water flowing from a thermostatic circulator. The system was placed close to the solenoid of a superconducting magnet which was horizontally oriented. Two cases were considered in the experiment: the first with the cooled wall close to the solenoid and the second with the heated wall close to the magnet's electric multi-wires. Natural convection was investigated for both cases: first without a magnetic field and second with various strengths of magnetic force acting on the system. The experimental results showed clearly suppression and enhancement of natural convection. Corresponding numerical computations were carried out for comparison with the experimental data. For this purpose, isotherms of the experimental data were extracted from the color images using the Particle Image Thermometry method and were compared with the numerical results.

Keywords: Natural convection; Magnetic field; Particle image thermometry; Numerical simulation; Flow visualization

1. Introduction

Extensive studies have been carried out on natural convection in enclosures. These include both experimental and numerical simulations. The earliest theoretical analysis of natural convection in an enclosure heated and cooled from sidewalls appears to be Batchelor [1]. He derived some features of the flow field and showed how to estimate the Nusselt number for convection. He also demonstrated that the flow is uniquely determined by three dimensionless parameters: the Rayleigh number, the Prandtl number and the aspect ratio. In 1961 Eckert and Carlson [2] reported some experimental results in a differentially heated cavity. They used interferometry to obtain the temperature field and local heat transfer. They also demonstrated that in tall slender cavities, the core is vertically stratified. The development of electronic computers in 1960s enabled the first numerical computation of the natural convection problem. One of the earliest models was introduced by Wilkes and Churchill [3] and de Vahl Davis [4]. In 1979, Jones [5] compared the steady state problem with the experiment. In 1980 Patterson and Imberger [6] portrayed the physical features of the development of natural convection in a differentially heated cavity by detailed scaling analysis. They were able to characterize different stages of the flow development including thermal boundary layer growth, the horizontal intrusion and attainment of the steady state.

In all the above-mentioned works on natural convection in enclosures, researchers were trying first to investigate the phenomena and later to enhance the heat transfer rates. The enhancement of heat transfer can be achieved using many methods, for example by placing fins on the heated wall, which was reported in [7]. Ozoe and his co-workers have studied the ef-

* Corresponding author. Tel.: +61 7 4781 5218; fax: +61 7 4781 6788.
E-mail address: tomasz.bednarz@jcu.edu.au (T. Bednarz).

1290-0729/$ – see front matter
doi:10.1016/j.ijthermalsci.2007.06.019

Nomenclature

$\vec{b}$	magnetic induction (b_x, b_y, b_z)	T
b_0	reference magnetic induction, $= \mu_m i/l = 1$–10 T	T
$\vec{B}$	dimensionless magnetic induction, $\vec{b}/b_0 = (B_x, B_y, B_z)$	
C	dimensionless momentum parameter for paramagnetic fluid, $= (1 + 1/(\beta\theta_0))$	
$\vec{e}_z$	unit vector in the vertical direction	
g	gravitational acceleration	$\mathrm{m\,s^{-2}}$
i	electric current in coil	A
l	length of the cubical enclosure	m
$m_{\mathrm{H_2O}}$	mass of water	kg
m_{glyc}	mass of glycerol	kg
m_{gado}	mass of gadolinium nitrate hexahydrate	kg
p	pressure	Pa
p_0	reference pressure, $= \rho_0\alpha^2/l^2$	Pa
P	dimensionless pressure, $= p/p_0$	
Pr	Prandtl number, $= \nu/\alpha$	
Ra	Rayleigh number, $= g\beta(\theta_h - \theta_c)l^3/(\alpha\nu)$	
t	time	s
t_0	reference time, $= l^2/\alpha = 10138.6$ s	s
T	dimensionless temperature, $= (\theta - \theta_0)/(\theta_h - \theta_c)$	
$\vec{u}$	velocity vector (u, v, w)	$\mathrm{m\,s^{-1}}$
u_0	reference velocity, $= \alpha/l$	$\mathrm{m\,s^{-1}}$
$\vec{U}$	dimensionless velocity vector, $= \vec{u}/u_0 = (U, V, W)$	
x_0, y_0, z_0	reference lengths, $= l = 0.032$ m	m
x_c	distance between center of the cube and center of the solenoid	m
X_c	non-dimensional distance between center of the cube and center of the solenoid, $= x_c/x_0$	
X, Y, Z	$= x/x_0, y/y_0, z/z_0$	

Greek symbols

α	thermal diffusivity	$\mathrm{m^2\,s^{-1}}$
β	thermal expansion coefficient	$\mathrm{K^{-1}}$
γ	dimensionless gamma parameter, $= \chi_0 b_0^2/(\mu_m g l)$	
λ	thermal conductivity	$\mathrm{W\,m^{-1}\,K^{-1}}$
μ_m	magnetic permeability	$\mathrm{H\,m^{-1}}$
ν	kinematic viscosity	$\mathrm{m^2\,s^{-1}}$
θ	temperature	K
θ_0	average temperature, $= (\theta_h + \theta_c)/2$	K
θ_c	temperature of cooled wall	K
θ_h	temperature of heated wall	K
ρ	density	$\mathrm{kg\,m^{-3}}$
ρ_0	reference density at temperature θ_0	$\mathrm{kg\,m^{-3}}$
τ	dimensionless time, $= t/t_0$	
χ	mass magnetic susceptibility	$\mathrm{m^3\,kg^{-1}}$
χ_m	volumetric magnetic susceptibility, $= \chi \cdot \rho$	

Subscripts

0	reference point
c	cold
gado	gadolinium nitrate hexahydrate
glyc	glycerin
h	hot
$\mathrm{H_2O}$	water

fects of magnetic field on various convective phenomena [8, 9]. Previously, Bednarz et al. have shown how to enhance the heat transfer by the application of a magnetic field [10]. It was achievable due to the recent development of super conducting magnets and the application of the magnetic force. Tagawa et al. [8] derived a model equation for magnetic convection using a method similar to the Boussinesq approximation and carried out numerical simulations in a cubic cavity. Kaneda et al. [9] studied the effect of a gradient magnetic field with a four-pole electric magnet. They placed a cubic enclosure filled with air inside the magnetic field and heated the air from above and cooled it from below at the center of the four-pole magnet. The stagnant conduction of air in the cube was disturbed and the convection of air was visualized with incense smoke, which was injected downwards from the center of the hot top plate toward the cold bottom plate, opposing the gravitational buoyancy force. This peculiar behavior of air agreed well with their corresponding numerical analysis. More information about magnetic convection and its application can be found in the book of Ozoe [11].

The present paper considers the magnetic field as a mechanism to change the character of the convective motion of a paramagnetic fluid in a cubic cavity heated from one vertical wall and cooled from the opposite wall. It is a supplement to the investigation reported in [10], in which heat transfer measurements with a 5-Tesla super-conducting magnet were presented and enhancement of convection heat transfer was reported. The present paper shows improved visualization experiments for the corresponding case with a 10-Tesla super-conducting magnet. It also shows an additional case where the convective flow is suppressed by the magnetic field.

2. The working fluid

In the present experiment an 80% mass aqueous glycerol solution was used as the working fluid. A mixture of water and glycerol is diamagnetic (both fluids are diamagnetic and have a negative magnetic susceptibility); therefore the solution was additionally mixed with crystals of gadolinium nitrate hexahydrate [$\mathrm{Gd(NO_3)_3{\cdot}6H_2O}$] to make it paramagnetic. Table 1 gives all measured data concerning the magnetic susceptibility of the 80% mass glycerol aqueous solution with different concentrations of gadolinium nitrate hexahydrate. The measurements were carried out at a temperature of 298 [K] with the Magnetic Susceptibility Balance *MSB,* based on the *Evan's method* [12].

The 0.8 [mol (kg of solution)$^{-1}$] concentration of $\mathrm{Gd(NO_3)_3{\cdot}6H_2O}$, which has a mass magnetic susceptibility $\chi = 23.0936 \times 10^{-8}$ [$\mathrm{m^3\,kg^{-1}}$], was chosen for further experiments. The work-

Table 1
Mass magnetic susceptibility data of 80% mass glycerol aqueous solution with different concentrations C_{gado} of gadolinium nitrate hexahydrate

m_{H_2O} [kg]	m_{glyc} [kg]	m_{gado} [kg]	C_{gado} [mol kg^{-1}]	ρ [kg m^{-3}]	$\chi \times 10^8$ [m^3 kg^{-1}]	$\Delta\chi \times 10^8$ [m^3 kg^{-1}]
0.00000	0.04370	0.00000	0.00	1253	−0.7403	0.0045
0.01072	0.04365	0.00432	0.16	1246	4.0687	0.0441
0.01090	0.04368	0.00966	0.33	1294	9.3184	0.0410
0.01068	0.04370	0.01627	0.51	1356	14.3300	0.0383
0.01068	0.04370	0.02469	0.69	1418	20.1899	0.0354
0.01067	*0.04373*	*0.03080*	*0.80*	*1463*	*23.0936*	*0.0290*
0.01068	0.04370	0.03595	0.88	1491	25.7915	0.0375
0.01070	0.04369	0.04477	1.00	1546	29.1874	0.0280

ing fluid was always prepared to have 0.03080 [kg] of gadolinium nitrate hexahydrate (molar mass 0.4514 [kg mol^{-1}]), 0.04373 [kg] of pure glycerol and 0.01068 [kg] of water (the values of m_{H_2O} and m_{glyc} listed in Table 1 may differ slightly due to minor measurement errors). In order to visualize the temperature field, a very small amount of thermo-chromic liquid crystal slurry (*KWN-20/25, Japan Capsular Product Inc.*) was added to the fluid (the visualization technique will be described later in this paper).

The density of the working fluid was measured by a pycnometer (*Brand 25 ml*) and has a value of $\rho = 1463$ [kg m^{-3}]. The viscosity at 298 [K] was measured with the Ostwald's viscosimeter as $\mu = 86.89 \times 10^{-3}$ [Pa s]. The thermal expansion coefficient was calculated based on the measurements of the fluid density at different temperatures from the definition ($\beta = -\frac{1}{\rho}\frac{\partial\rho}{\partial T}$) and has a value of $\beta = 0.52 \times 10^{-3}$ [K^{-1}] within the range of the experimental temperatures. The thermal conductivity ($\lambda = 0.397$ [W m^{-1} K^{-1}]) and the thermal diffusivity ($\alpha = 1.01 \times 10^{-7}$ [m^2 s^{-1}]) were estimated from [13]. The Prandtl number was calculated to be $Pr = 584$.

3. Experimental setup

The experimental apparatus is shown in Fig. 1. Five separate elements were designed to assemble the final experimental model. Those are: two copper plates (one for the cooling side and the other for the heating side) with three holes in each to place six T-type thermocouples; a Plexiglas cubic cavity with a filling hole; and cooling and heating chambers also made of Plexiglas. One copper plate was heated by a nichrome wire covered by rubber wound in the heating chamber. This wire was connected to a DC power supply (*Kikusui PAK 60-12A*). The opposite copper wall was cooled by water pumped from a circulator (*RK20 KS LAUDA*). The cubic cavity had an internal dimension of 0.032 [m] on each side.

When all parts of the experimental setup were assembled, it was possible to fill the enclosure with the working fluid. This was done with a syringe and a thin needle. When the enclosure was filled, the hole in the wall was sealed by silicone resin and the experimental apparatus was placed just outside of the bore of the 10-Tesla super-conducting magnet.

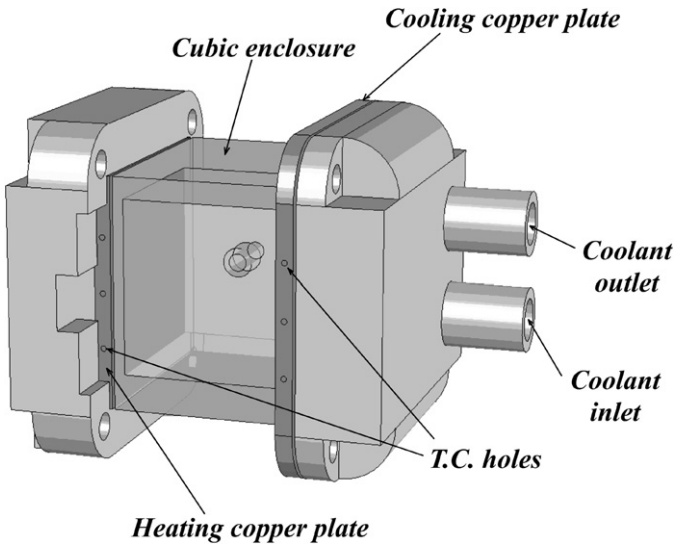

Fig. 1. Experimental apparatus.

4. The cases considered

The present paper considers two experimental cases. In both cases the same 10-Tesla super-conducting magnet was oriented horizontally. In Case 1 the location of the solenoid is close to the heated wall and in Case 2 the location of the solenoid is close to the cooled wall. Furthermore, the experimental model was placed just outside of the bore of the magnet to allow undisturbed flow visualization. In our previous experiment [10], we used a similar configuration for Case 1. However, the enclosure was initially located inside the bore of a 5-Tesla super-conducting magnet. In order to photograph the temperature field we had to remove the model from the bore and place it gently on a stand. It was the only possible way to visualize the flow with that magnet as the magnetic field outside of the bore was too weak to drive any convection. However, using the 10-Tesla super-conducting magnet in the present study, it is possible to see clearly how the magnetic convection works inside the cavity when the cavity itself is placed just outside the bore. Therefore, we decided to repeat the previous experiment (Case 1) with the 10-Tesla magnet for the purpose of visualization. In addition, we also consider one additional experimental case (Case 2) in the present paper which was not reported before.

5. Visualization

Visualization of the temperature field was possible due to the addition of a very small amount of thermo-chromic liquid crystal slurry (*KWN-20/25*) to the working fluid. The liquid crystals reflect a definite color at a specific temperature and a specific viewing angle. Therefore, as seen in Fig. 2, a mirror was placed above the enclosure to reflect the white light coming from a projector lamp located at a distance around 3 [m] from the mirror. In this way, the vertical middle cross-section of the cube was illuminated giving a color map of the temperature field. All experimental images were taken by a digital camera (*Canon EOS 10D + EF70-200 mm f2.8*) after a steady state was attained for each case. All pictures from the experiment were shot

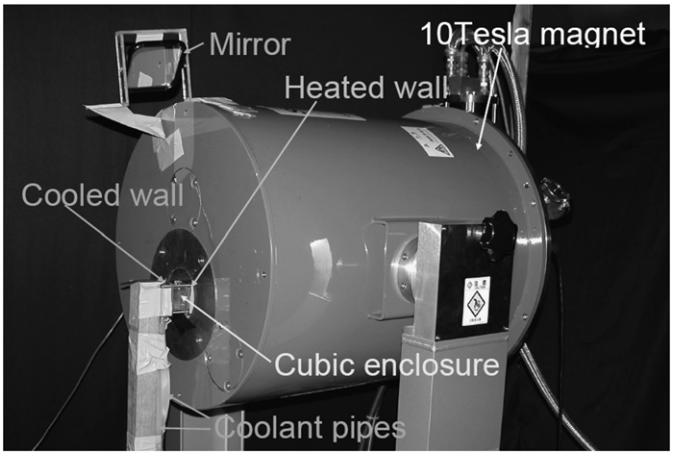

Fig. 2. Photograph of the enclosure position in the experiment (*Case 1*).

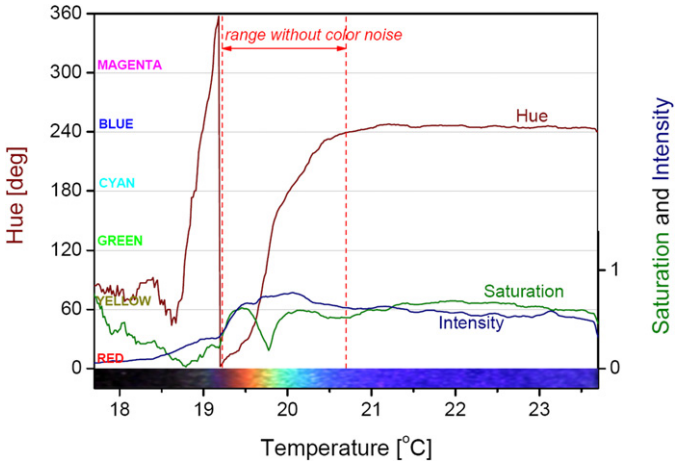

Fig. 3. Variation of hue, saturation and intensity with temperature (data from conduction experiment).

in the RGB (Red, Green, Blue) color model with a 12-bit resolution (RAW mode) for each color component. In order to get quantitative information from the recorded pictures, the Particle Image Thermometry (PIT) technique was adopted. It is a non-invasive method of temperature measurements. The temperature information comes from post-processing of the true-color images of the liquid crystal patterns, and the method itself is relatively simple. It is a valuable tool for the verification and validation of numerical results.

Calibration of the color map is required. At first, a conduction experiment, heated from above and cooled from below, was carried out with the same experimental apparatus to obtain a color map of the temperature. Having a color picture from such experiment, the RGB color values were converted to an HSI (Hue-Saturation-Intensity) color model by the following formulae:

$$H = 90 - \arctan\left(\frac{2R - G - B}{\sqrt{3}(G - B)}\right) + \begin{cases} 0 & \text{for } G > B \\ 180 & \text{for } G < B \end{cases} \tag{1}$$

$$S = \frac{\mathrm{Max}(R, G, B) - \mathrm{Min}(R, G, B)}{\mathrm{Max}(R, G, B)} \tag{2}$$

$$I = \frac{\sqrt{R^2 + G^2 + B^2}}{\sqrt{3}} \tag{3}$$

where the hue (H) represents the color, the intensity (I) represents the physical brightness and the saturation (S) represents the purity of the color.

Fig. 3 shows the plots of hue, intensity and saturation versus the temperature from the conduction experiment. Along the left-hand side coordinate, the hue values and corresponding color names are listed. The variation in hue between 19.2 and 20.7 °C increases monotonically, and the usable temperature range of the liquid crystals is therefore limited to this temperature range. A measurement of hue in this range therefore may be directly converted to a measurement of temperature.

6. Numerical model

Corresponding numerical computations were carried out for the experimental cases. The numerical model for the magnetic convection of a paramagnetic fluid is based on the work of Tagawa et al. [8]. It employs Curie's law under which the magnetic susceptibility of paramagnetic substances is inversely proportional to its absolute temperature. For not very large temperature differences, the magnetic susceptibility may be represented by a Taylor expansion and the magnetic term in the momentum equation becomes proportional to the temperature T based on the approach presented in [8]. When a temperature difference occurs in the paramagnetic fluids, a magnetic buoyancy force is generated in the presence of a magnetic field. Examples of our previous computations on the same topic can be found in [8–11].

The governing equations in non-dimensional forms are defined as follows:

Continuity equation

$$\vec{\nabla} \cdot \vec{U} = 0 \tag{4}$$

Momentum equation

$$\frac{D\vec{U}}{D\tau} = -\vec{\nabla} P + Pr\,\nabla^2 \vec{U} + Ra\,Pr\,T\left[\vec{e}_z - \gamma \frac{C}{2}\vec{\nabla} B^2\right] \tag{5}$$

Energy equation

$$\frac{DT}{D\tau} = \nabla^2 T \tag{6}$$

The computational parameters were defined as follows:

- Prandtl number

$$Pr = \frac{\nu}{\alpha} = 100 \tag{7}$$

- Momentum parameter for paramagnetic fluids

$$C = 1 + \frac{1}{\beta\theta_0} = 7.56 \tag{8}$$

- Rayleigh number

$$Ra = \frac{g\beta l^3(\theta_h - \theta_c)}{\alpha\nu} = 28040 \cdot \Delta\theta \tag{9}$$

- Gamma parameter

$$\gamma = \frac{\chi_0 b_0^2}{\mu_m g l} = 0.586 \cdot b_0^2 \tag{10}$$

Non-dimensionalization was done using the following formulae:

$$X = x/x_0, \quad Y = y/y_0, \quad Z = z/z_0, \quad U = u/u_0$$
$$V = v/v_0 \quad W = w/w_0 \quad \tau = t/t_0, \quad P = p/p_0$$
$$\vec{B} = \vec{b}/b_0, \quad T = (\theta - \theta_0)/(\theta_h - \theta_c), \quad x_0 = y_0 = z_0 = l$$
$$u_0 = v_0 = w_0 = \alpha/l, \quad t_0 = l^2/\alpha$$
$$b_0 = \mu_m i/l, \quad p_0 = \rho_0 \alpha^2/l^2$$

It should be mentioned here that the steady flow characteristics are almost independent of the *Pr* number for higher Prandtl number fluids ($Pr > 10$) which has been confirmed in preliminary computations (for $Pr > 10$ the effect of inertia is negligible). Therefore, in this case the *Ra* number becomes the unique parameter to characterize the buoyant convection in the absence of a magnetic field. A similar comparison was reported by Shyy and Chen [14]. It should be mentioned that the transient state however, may differ depending on the Prandtl number. In this study, we arbitrarily chose $Pr = 100$ for the simulations. This shortened the time needed for convergence to steady state in the numerical simulations.

Distribution of the magnetic field was computed using the Biot–Savart's law for a multi-coil system (the 10-Tesla superconducting magnet has two solenoids, *Sumitomo Heavy Industries Ltd.*).

The boundary conditions for this system were as follows:

$U = V = W = 0$ at all walls of the cube
$T = 0.5$ at $X = -0.5$
$T = -0.5$ at $X = 0.5$
$\partial T/\partial Y = 0$ at $Y = -0.5, 0.5$
$\partial T/\partial Z = 0$ at $Z = -0.5, 0.5$

A conduction state was arbitrarily selected as an initial condition.

$$U = V = W = 0, \quad T = -X \quad \text{where } -0.5 \leqslant X \leqslant 0.5$$

The average Nusselt number was computed on the hot wall from the following definition:

$$Nu = \frac{\int_{-0.5}^{0.5}\int_{-0.5}^{0.5} (\partial T/\partial X)_{X=-0.5}^{\text{convection}} \, \mathrm{d}Y \, \mathrm{d}Z}{\int_{-0.5}^{0.5}\int_{-0.5}^{0.5} (\partial T/\partial X)_{X=-0.5}^{\text{conduction}} \, \mathrm{d}Y \, \mathrm{d}Z} \tag{11}$$

The normalized governing equations were approximated with a finite difference method. The Highly Simplified Marker And Cell method was used to iterate mutually the pressure and velocity fields. The inertial terms were approximated using the UTOPIA scheme [15]. The grid number employed was $40 \times 40 \times 40$. A grid dependency test for the same model equations was reported in [16] which showed that the effect of the grid size was insignificant comparing with a mesh of $30 \times 30 \times 30$.

7. Results and discussion

In the experiment, as indicated above flow visualization was made with a 10-Tesla super-conducting magnet with the experimental apparatus placed just outside the bore of the magnet. Fig. 4 shows the cross-sectional schematic views of the system used in the numerical simulations for both cases: *Case 1* and *Case 2*. All dimensions in the figure are non-dimensionalized. The center of the enclosure is placed at a distance of $X_c = 7.28$ from the center of the solenoid which corresponds to a distance of 0.233 [m] in the real experiment. In Fig. 4(a), the hot wall on the right is placed close to the horizontally oriented system of the coils. Fig. 4(b) shows the configuration for *Case 2*. In the enclosure of Fig. 4, schematic vectors of the gravitational and magnetic forces are shown. The gravitational force points always downwards. Under the effect of the gravitational force, hot fluid with a lower density tends to go upwards and cold fluid with a higher density tends to go downwards in comparison to the fluid at the average temperature. To indicate this clearly, the force vectors near the hot wall are shown to be

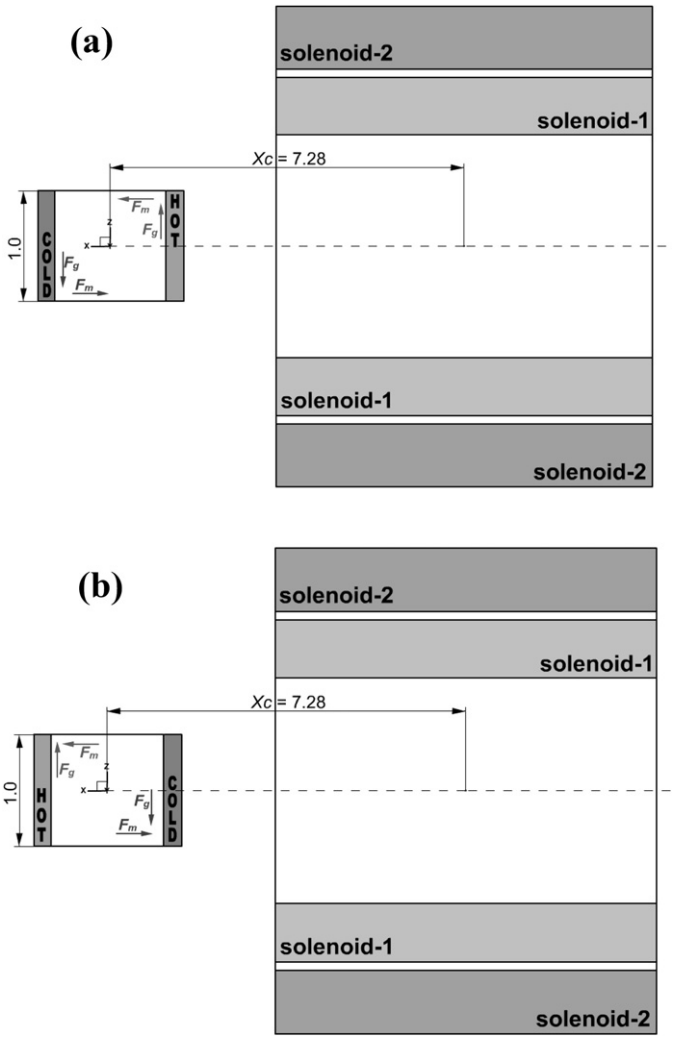

Fig. 4. Schematic view of the cross-section of the system with 10-Tesla superconducting magnet (a) *Case 1*, (b) *Case 2*. F_m denotes the magnetic buoyancy force and F_g, the gravitational buoyancy force acting on the fluid.

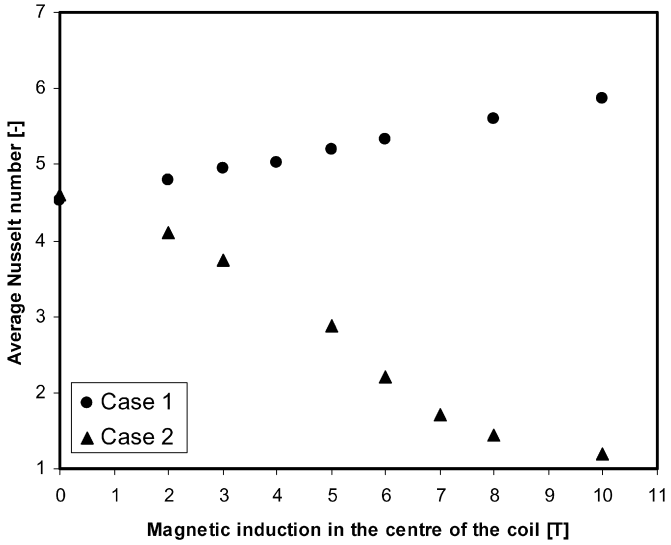

Fig. 5. The average Nusselt numbers for *Case 1* and *Case 2*.

directed upwards and the ones near the cold wall downwards. Similarly, the magnetic force attracts paramagnetic fluids. However, hot fluid has smaller value of magnetic susceptibility and is attracted less by the magnet; whereas cold fluid has larger values of magnetic susceptibility and is attracted more. To indicate this, the force vectors F_m near the cold wall are shown to be directed towards the magnet and those near the hot wall away from the magnet, in contrast with the fluid at the average temperature.

Fig. 5 shows the average Nusselt numbers calculated numerically for both cases. The Nusselt numbers are plotted versus the maximum magnetic induction measured at the center of the solenoids system. In *Case 1*, the average Nusselt number increases with the strength of the magnetic field—the natural convection is enhanced. In *Case 2* however, the increase of the magnetic field strength causes natural convection to be increasingly suppressed. This is clearly illustrated by the plot of the average Nusselt numbers for *Case 2* which becomes close to the unity at 10 T. It means that the convective motion becomes very weak and conduction dominates in the system. Convection is suppressed and gravitational effect is overcome by the magnetic field.

Since the experiment with 10-Tesla super-conducting magnet was carried out only for the visualization purposes, corresponding heat transfer measurements were not available at this time. Experimental heat transfer measurements with a well insulated cubical cavity however were already presented in our previous paper [10]. In that study, a separate experiment was then carried out with the enclosure thermally insulated, and placed in the bore of 5-Tesla super-conducting magnet. It has shown good agreement with the corresponding numerical simulations.

7.1. Case 1

Fig. 6 shows the resultant force vectors in three horizontal cross-sections and the long-time streak lines for three nominal strengths of the magnetic field corresponding to the experimental data. The nominal strength of the magnetic induction at the solenoid centre are 0, 5 and 10 [T], respectively, and the actual strengths at the centre of the enclosure are computed to be 0, 0.66 and 1.32 [T], respectively. The corresponding dimensionless magnetic strengths are $\gamma = 0$, 14.65 and 58.6, respectively. The experimental Rayleigh numbers were $Ra = 9.16 \times 10^4$, 8.83×10^4 and 8.26×10^4 and those numbers were also used for numerical simulations. The force vectors are computed as the sum of the magnetic and gravitational buoyancy forces and their non-dimensional magnitudes are denoted by numbers above the arrows drawn in each figure. The long-time streak lines were obtained based on the actual velocity field by tracking massless particles.

At the magnetic induction of 0 [T], the magnetic buoyancy force is not acting and pure gravitational natural convection can be observed. The force vectors over the hot wall are directed upwards and those near the left-hand side cold wall are directed downwards. In the upper part of the enclosure the relatively hot fluid prevails, and the force vectors are directed upwards in contrast to the lower part of the enclosure where the forces are directed downwards where the fluid is relatively colder. As a result, a large roll is generated as seen from the long-time streak lines. The hot fluid travels up the heated wall and then along the top ceiling toward the cold wall. Relatively colder fluid travels down the cold wall and then proceeds along the bottom adiabatic wall toward the hot wall.

At the magnetic induction of 5 [T], due to the attracting effect for the relatively colder fluid (with a larger value in the mass magnetic susceptibility for a paramagnetic fluid), the force vectors are directed toward the magnet. In contrast the hotter fluid is moved away from the magnet.

At the magnetic induction of 10 [T] the force vectors become almost horizontal. The cold fluid is strongly attracted toward the solenoid while the hot fluid is moving away as indicated by those vectors. This can be clearly seen in the regions close to both vertical isothermal walls. The long time streak-lines are also affected by the magnetic field. The general direction of the flow is the same, but the flow itself is stronger. These can be seen more clearly from the isotherms shown in the next set of figures.

Fig. 7 shows vertical cross-sections of the temperature fields. In this figure, the experimental images along with the isotherms obtained with the PIT (Particle Image Thermometry) method are shown on the left, whereas the numerically computed temperature contours are shown on the right. At a magnetic induction of 0 [T], the usual natural convection temperature structures can be observed. An increase of the strength of the magnetic field causes stronger convection. It is seen in Fig. 7 that the thicknesses of the boundary layers above the floor and below the ceiling decreases with the increase of the magnetic strength, suggesting stronger circulation. At a magnetic induction of 10 [T], clear thermal tongues are observed close to the cold and hot walls. It is seen in Fig. 7 that the temperatures extracted from the experimental pictures agree well with the numerical results.

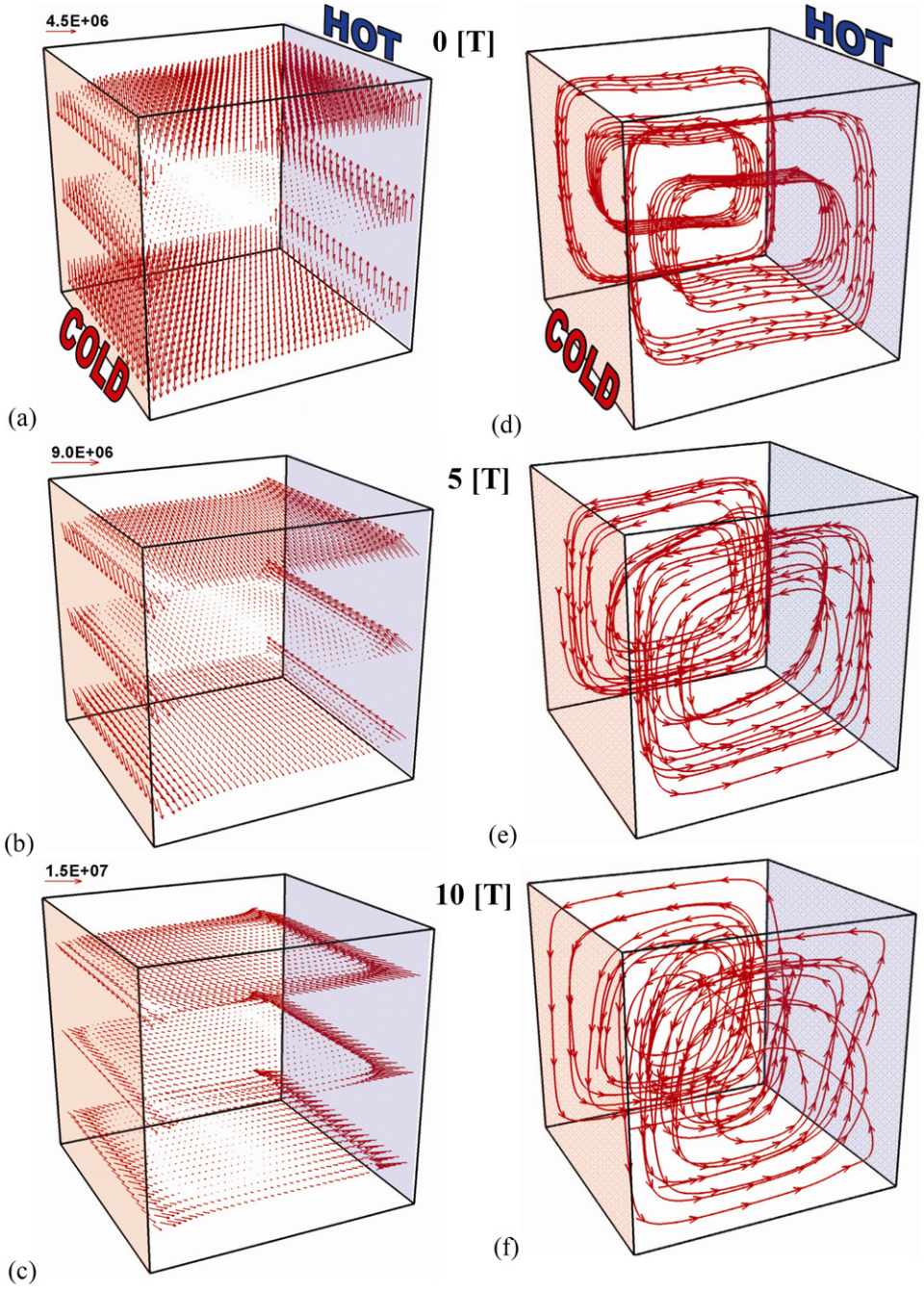

Fig. 6. Force vectors (left) and long time streak lines (right) for *Case 1*.

7.2. *Case 2*

Fig. 8 shows the computed vectors and long-time streak lines for three nominal strengths of the magnetic field with the second configuration. The computed Rayleigh numbers are $Ra = 9.63 \times 10^4$, 1.15×10^5 and 1.48×10^5, respectively. Again, the force vectors here are estimated as the summation of the magnetic and gravitational buoyancy forces—their dimensionless magnitudes are denoted by numbers above the specific plot. The results are computed at the nominal strength of the magnetic induction at the solenoid centre, which is at 0, 5 and 10 [T], respectively. The actual strengths at the centre of the enclosure are computed as 0, 0.66 and 1.32 [T], respectively, and the corresponding dimensionless magnetic strengths are $\gamma = 0$, 14.65 and 58.6, respectively.

At the magnetic induction of 0 [T], pure gravitational convection can be observed. Only the gravitational buoyancy force acts vertically along the hot and cold walls as indicated by the vectors, and a large convective cell is generated over the entire flow domain. Four streak lines represent a circulation in the horizontal direction due to the double spiral flow observed by Ozoe et al. [17].

At the magnetic induction of 5 [T], due to the "repelling" effect for the hotter fluid (with a smaller value in the mass

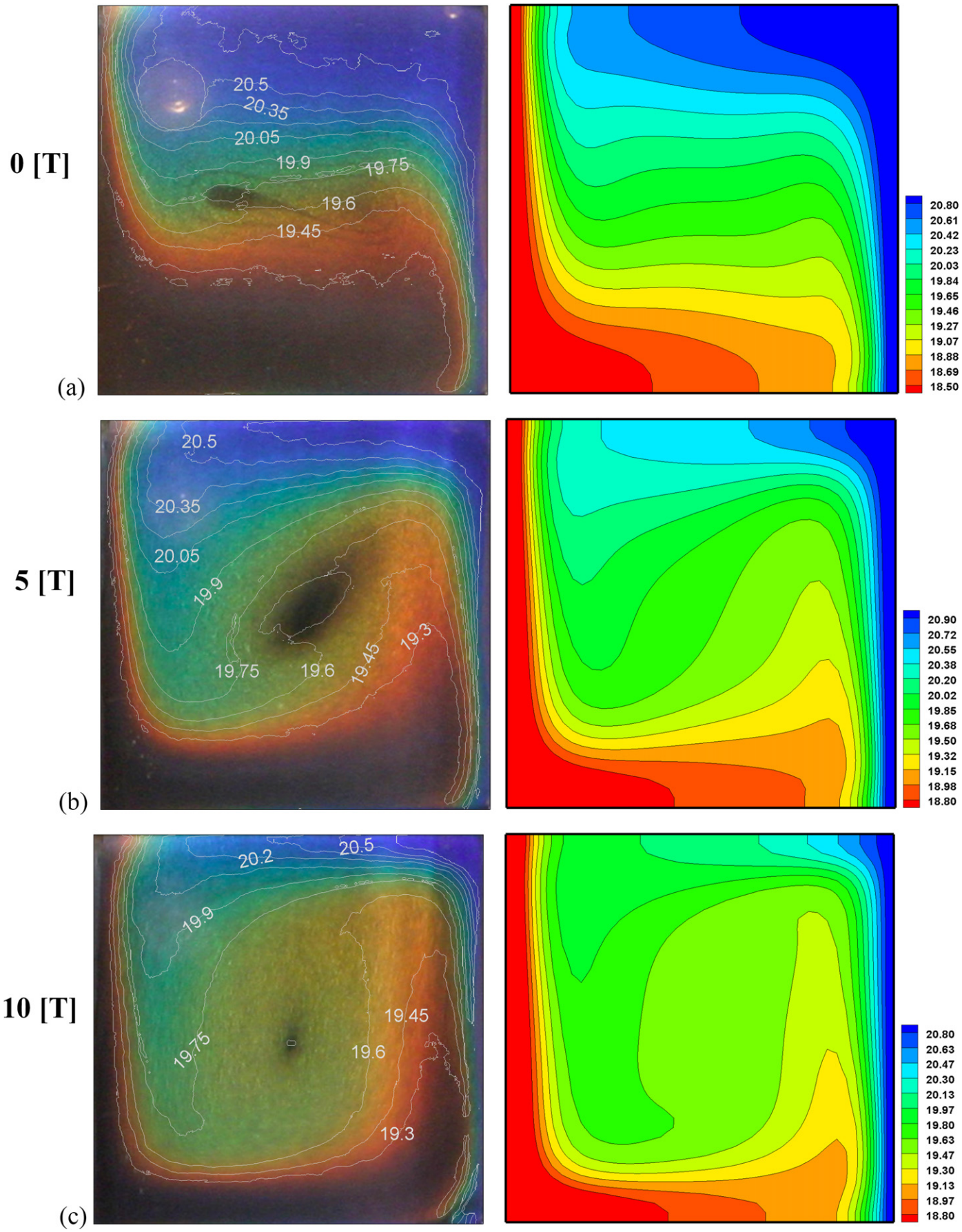

Fig. 7. Isotherms, *Case 1*. Left: experiment + PIT, right: numerical simulations.

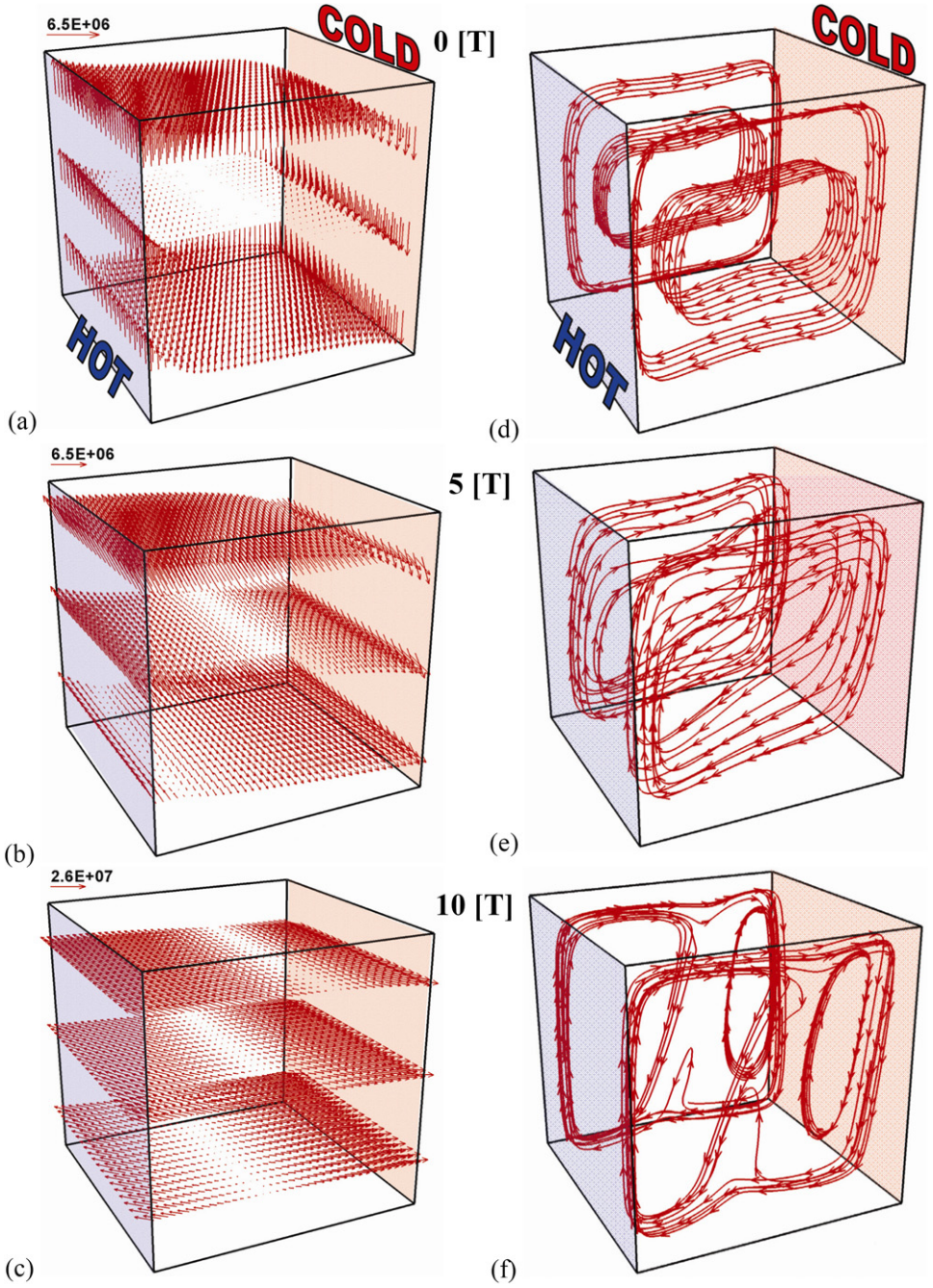

Fig. 8. Force vectors (left) and long time streak lines (right) for *Case 2*.

magnetic susceptibility for paramagnetic fluid), the vectors are directed further away from the magnet, which is placed on the cold wall side. However, the cold fluid is subject to an attracting force from the magnet and the vectors are directed toward the magnet. The long time streak lines are also affected by the additional magnetic field and the convection differs noticeably from that of the pure gravitational convection.

At the magnetic induction of 10 [T], the magnetic buoyancy force becomes dominant and the force vectors are directed almost horizontally. The streak lines become quite complicated. Generally speaking, bulk convection between the cold and hot walls exists; but the fluid convection is roughly separated between the cold and hot region. This convection transfers only a small amount of energy between the hot and cold walls, and the system is in a typical mode similar to a conduction state. These aspects can be seen more clearly from the isotherms shown in Fig. 9.

Fig. 9(a) shows a photograph of the liquid crystal patterns, overlaid with isotherms computed from the PIT process at a mid-vertical plane of the enclosure at the magnetic induction of 0 [T]. The left side wall is heated and the right side wall is cooled. Since the walls are made of copper plate in the experiments, the isothermal condition is well satisfied. These isotherms are typical for pure natural convection in the clock-

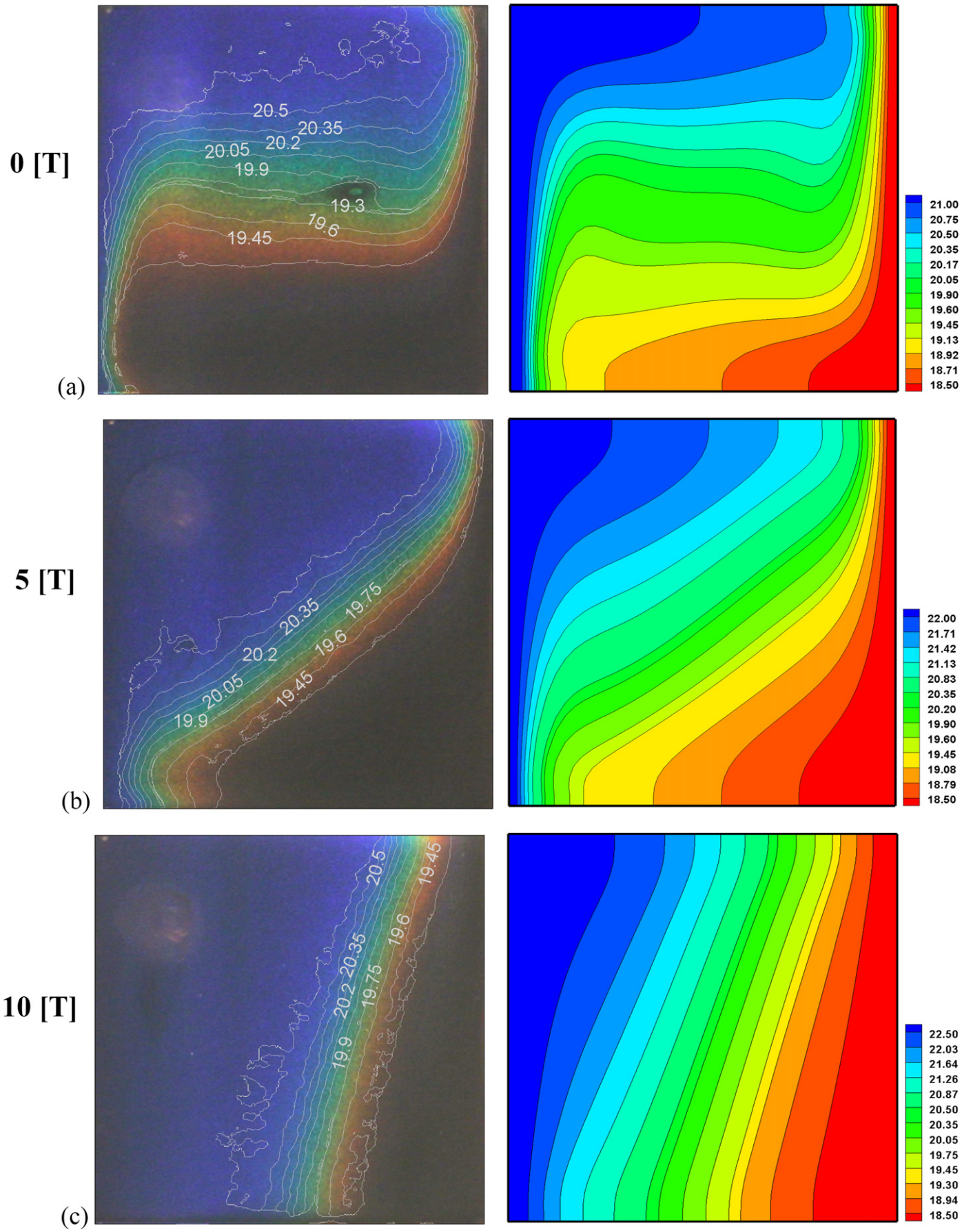

Fig. 9. Isotherms, *Case 2*. Left: experiment + PIT, right: numerical simulations.

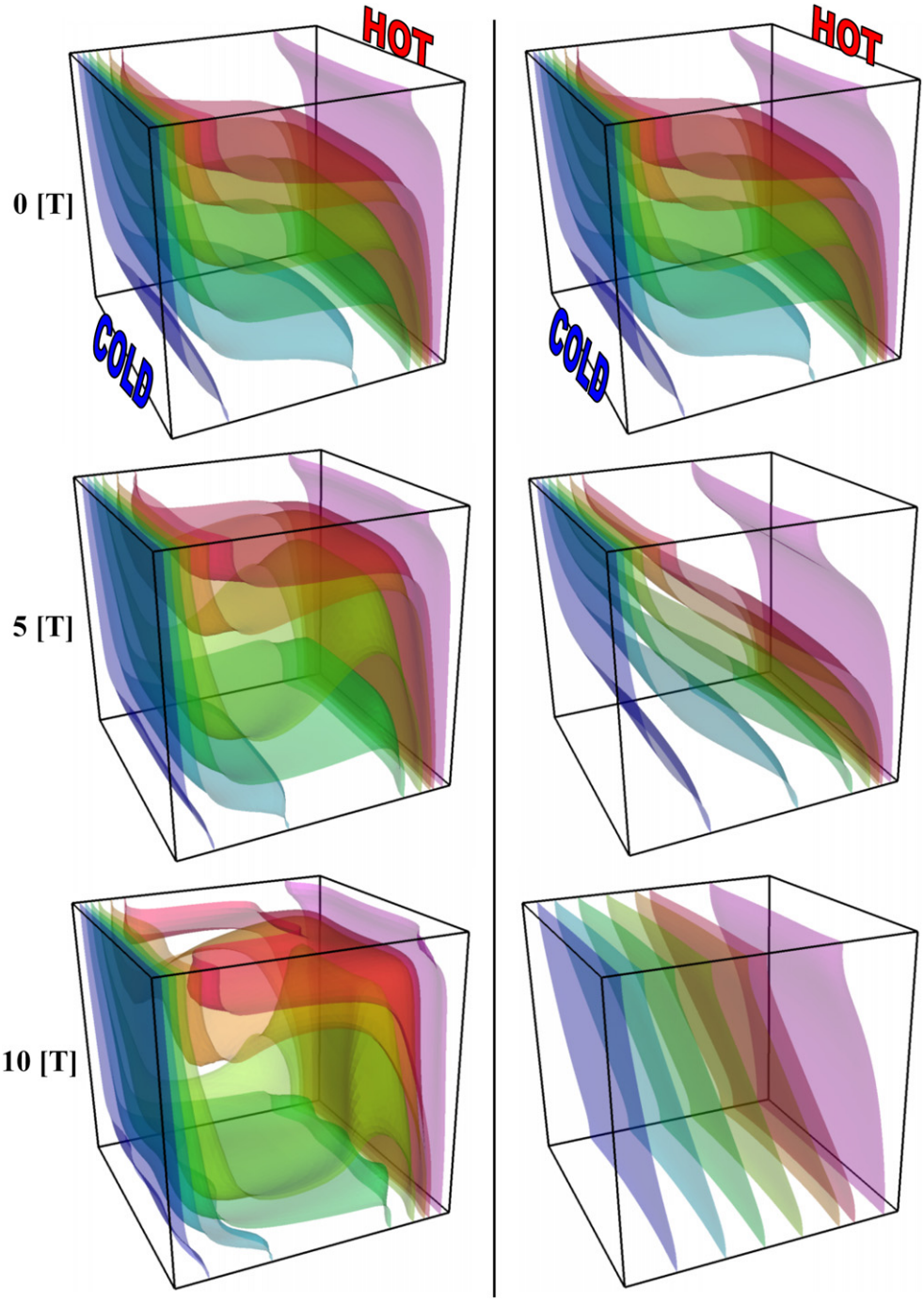

Fig. 10. Isothermal surfaces for *Case 1* (left) and *Case 2* (right).

wise direction with a thermal stratification in the core region, and a quasi two-dimensional mode is established. The right picture shows the isotherms at the mid-vertical plane computed from the three-dimensional numerical analyses. It is seen in Fig. 9(a) that the experimental and numerical isotherms match quite well with each other.

Fig. 9(b) shows the results obtained at the magnetic induction of 5 [T]. The isotherms become more inclined and the corresponding numerical isotherms show similar features.

Fig. 9(c) shows the results at the magnetic induction of 10 [T]. It is seen in this figure that the isotherms become almost vertical, indicating a conduction-like situation. Again, the corresponding numerical results are consistent with the experimental data.

7.3. *Effect of the front and rear walls*

Fig. 10 shows the isothermal surfaces for both cases: *Case 1* and *Case 2*, with colors of all pictures adjusted for clear visibility of the temperature patterns. The purpose of this figure is to show three-dimensional flow characteristics and the effect of the walls on the spatial temperature distribution in both

cases. At 0 T, both cases have the usual natural convection profiles which can be assumed to be almost two dimensional in the analysis. In the regions very close to the front and rear walls, delicate curling is observed and is caused by the non-slip boundary condition. Increasing the strength of the magnetic field changes the temperature distribution characteristics. It is seen in Fig. 10 that *Case 1* becomes more three dimensional when the magnetic strength is increased. However *Case 2* becomes even more two dimensional due to the weakening convection effect. In *Case 1*, at 10 T three-dimensional effects are easily observed, for instance along the top horizontal edges where hot fluid moves toward the cold wall is squeezed out to the sides by the relatively colder fluid.

8. Conclusions

Experiments and numerical computations were carried out for natural convection of a paramagnetic fluid in a cubic enclosure heated and cooled from opposing vertical walls with four other walls thermally insulated. The computed conditions were taken from the accompanying flow visualization experiment and the computed isotherms agree well with the observed ones for the aqueous glycerol solution with the dissolved gadolinium nitrate hexahydrate. The good agreement between the experimental and numerical isotherms strongly suggests that the present numerical model can be applied to modeling such type of experiments with confidence.

It is worth noting that the configuration of Case 1 in the present experiments is similar to the experiment reported in [10], which suffered a deficiency in the experimental procedures due to limitations of the experimental system in that case. The previous experiment was carried out with a 5-Tesla super-conducting magnet, and the experimental model had to be placed inside the bore of the magnet in order to have a sufficiently strong magnetic field. Once a steady state condition was achieved, the enclosure was then taken out from the bore of the magnet for photographing purpose. Unfortunately, that was the only possible way to visualize the flow at that time due to the limitations of the magnet. Although the previous experimental results clearly showed similar enhancement of natural convection, they were strongly influenced by the gravity force [10]. This is because the magnetic force acting on the fluid was reduced significantly when the model was taken out of the bore despite that this procedure happened within a very short time. As a consequence, a disturbed picture of what was actually happening in the enclosure was recorded; the thermal tongues observed in the present experiments were not clearly visible in the previous experiment, and direct comparison with numerical simulation was not possible then.

With the 10-Tesla strong magnet, we have repeated the same experiment in the present study without disturbing the flow. In this experiment, the experimental cube was placed just outside the bore, and the magnetic field was strong enough to drive the convective motion. The visualization was made properly without any disturbances to the flow field, and thus the obtained experimental results compare favorably with the numerical simulations. Also it should be mentioned, that no instabilities were observed in experimental and numerical results.

Acknowledgements

The authors gratefully acknowledge the financial support of the Australian Research Council. Also, a part of this work was supported by Grant AGH-UST No. 11.11.180.375.

References

[1] G.K. Batchelor, Heat transfer by free convection across a close cavity between vertical boundaries at different temperatures, Quarterly Journal of Applied Mathematics 12 (1954) 209–233.
[2] E.R.G. Eckert, W.O. Carlson, Natural convection in an air layer enclosed between two vertical plates with different temperatures, International Journal of Heat and Mass Transfer 2 (1961) 106–120.
[3] J.O. Wilkes, S.W. Churchill, The finite-difference computation of natural convection in a rectangular enclosure, AIChE Journal 12 (1966) 161–166.
[4] G. de Vahl Davis, Laminar natural convection in an enclosed rectangular cavity, International Journal of Heat and Mass Transfer 11 (1968) 1675–1693.
[5] I.P. Jones, A numerical study of natural convection in an air-filled cavity: comparison with experiment, Numerical Heat Transfer 2 (1979) 193–213.
[6] J.C. Patterson, J. Imberger, Unsteady natural convection in a rectangular cavity, Journal of Fluid Mechanics 100 (1980) 65–86.
[7] F. Xu, J.C. Patterson, C. Lei, Experimental observations of the thermal flow around a square obstruction on a vertical wall in a differentially heated cavity, Experiments in Fluids 40 (2006) 364–371.
[8] T. Tagawa, R. Shigemitsu, H. Ozoe, Magnetizing force modeled and numerically solved for natural convection of air in a cubic enclosure: Effect of the direction of the magnetic field, International Journal of Heat and Mass Transfer 45 (2002) 267–277.
[9] M. Kaneda, T. Tagawa, H. Ozoe, Convection induced by a cusp-shaped magnetic field for air in a cube heated from above and cooled from below, Journal of Heat Transfer 124 (2002) 17–25.
[10] T. Bednarz, E. Fornalik, T. Tagawa, H. Ozoe, J.S. Szmyd, Experimental and numerical analyses of magnetic convection of paramagnetic fluid in a cube heated and cooled from opposing vertical walls, International Journal of Thermal Sciences 44 (2005) 933–943.
[11] H. Ozoe, Magnetic Convection, Imperial College Press, ISBN 1-86094-578-3, 2005.
[12] Sherwood Scientific Ltd., Magnetic Susceptibility Balance Instruction Manual, second ed., Cambridge, 2001.
[13] D.R. Lide (Ed.), Handbook of Chemistry and Physics, 82 ed., Chemical Rubber Company Press, Boca Raton, FL, 2001–2002.
[14] W. Shyy, M.H. Chen, Effect of Prandtl number on buoyancy-induced transport processes with and without solidification, International Journal of Heat Mass Transfer 33 (11) (1990) 2565–2578.
[15] T. Tagawa, H. Ozoe, Effect of Prandtl number and computational schemes on the oscillatory natural convection in an enclosure, Numerical Heat Transfer A 30 (1996) 271–282.
[16] T. Bednarz, T. Tagawa, M. Kaneda, H. Ozoe, J.S. Szmyd, Numerical study of joint magnetisation and gravitational convection of air in a cubic enclosure with an inclined electric coil, Progress in Computational Fluid Dynamics 5 (3/4/5) (2005).
[17] H. Ozoe, N. Sato, S.W. Churchill, Experimental confirmation of the three-dimensional helical streaklines previously computed for natural convection in inclined rectangular enclosure, Int. Chem. Eng. 19 (3) (1979) 454–462.